Journal of Applied Physics

First principles investigation of charge transition levels in monoclinic, orthorhombic, tetragonal, and cubic crystallographic phases of HfO_2

Cite as: J. Appl. Phys. **129**, 084102 (2021); https://doi.org/10.1063/5.0033957
Submitted: 20 October 2020 • Accepted: 30 January 2021 • Published Online: 22 February 2021

Md Nur K Alam, S. Clima, B. J. O'Sullivan, et al.

Journal of Applied Physics ARTICLE scitation.org/journal/jap

First principles investigation of charge transition levels in monoclinic, orthorhombic, tetragonal, and cubic crystallographic phases of HfO_2

Cite as: J. Appl. Phys. **129**, 084102 (2021); doi: 10.1063/5.0033957
Submitted: 20 October 2020 · Accepted: 30 January 2021 ·
Published Online: 22 February 2021

Md Nur K Alam,[1,2,a] S. Clima,[1] B. J. O'Sullivan,[1] B. Kaczer,[1] G. Pourtois,[1,3] M. Heyns,[1,2] and J. Van Houdt[1,4]

AFFILIATIONS

[1]Institute for Microelectronics, IMEC 3001, Leuven, Belgium
[2]Department of Materials Engineering, KU Leuven 3001, Leuven, Belgium
[3]PLASMANT, University of Antwerp, 2610 Antwerpen, Belgium
[4]Department of Physics and Astronomy, KU Leuven, 3001 Leuven, Belgium

[a]**Author to whom correspondence should be addressed:** md.nur.kutubul.alam@imec.be and alamjhilam@eee.kuet.ac.bd

ABSTRACT

A first-principles study of native point defects in monoclinic, cubic, two different tetragonal, and five different orthorhombic phases of hafnia (HfO_2) is presented. They include vacancy of tri-coordinated and tetra-coordinated oxygen, metal vacancy, interstitial metal, and interstitial oxygen. Defect formation energy, trap depth, and relaxation energy upon optical excitation of defects are listed. The trap depth of oxygen vacancies shows little variation among different phases compared to other defects. Results of the trap depth are compared against measurements and found to have reasonable agreement.

I. INTRODUCTION

Hafnia (HfO_2) is probably the most important high-κ insulator in today's CMOS industry that has been introduced as a replacement for silicon-dioxide as the gate oxide of MOSFETs. The low temperature phase, i.e., the monoclinic (*m*) HfO_2, has been used in the CMOS gate stack for the last 10 years. Recently, a multitude of prospective applications of hafnia appeared, thanks to its multiple crystallographic phases that can be stabilized by tuning their growth conditions.[1] One of the phases that attracted attention is the metastable orthorhombic one that exhibits ferroelectricity. Its discovery opened the door for the exploration of ferroelectric (FE) capacitor for FE-RAM (analogous to DRAM), FE-FET for non-volatile-memory, etc. The metastable phase is stabilized by the doping of the oxide and/or strain engineering, etc.[2]

Each phase of HfO_2 has a thermodynamic "internal energy" at which it can be stabilized. With increasing temperature, the crystal changes its atomic structure from low energy toward higher energy phases. The transition generally follows the sequence: monoclinic (*m*)–orthorhombic (*o*)–tetragonal (*t*)–cubic (*c*). These phases are defined by crystallographic space group symmetry. Crystals with different lattice constants can have the same symmetry group and vice versa. This leads to the existence of many crystalline allotropes. In addition, each allotrope with a given symmetry (phase) can have many variants. In this study, we chose several low-energy *m*, *o*, and *t* HfO_2 systems. The *t* and *o* phases have two and five different variations, respectively. They were labeled *t1*, *t2*, and *o1*–*o5*. Both *o1* and *o2* have *Pbca* spacegroup symmetry with different lattice parameters. They are $10.169 \times 5.184 \times 5.297$ Å^3 and $5.086 \times 5.248 \times 10.059$ Å^3, respectively. Figure 1 compares the computed ground state energy of all the HfO_2 allotropes under study.

Reliability of hafnia based devices has always been a concern because of their high permeability to oxygen, the low crystallization temperature, and the formation of the low-k interfacial layer during high temperature processing.[3] Film annealing involves oxygen diffusion through the already grown oxide and the possible formation of interstitial oxygen.[4] Likewise, interstitial metal is also possible. Oxygen as well as metal vacancy can be present due to the breaking of chemical bonds. They can serve as a charge trapping center,

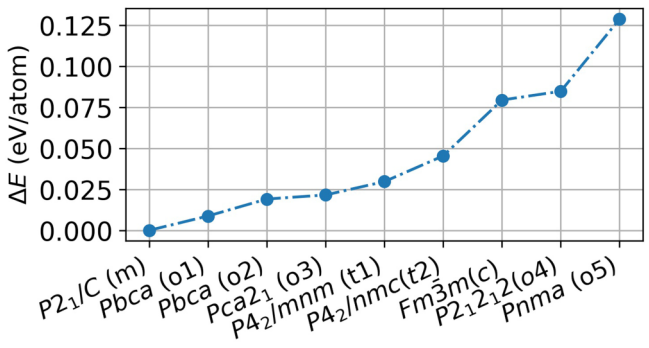

FIG. 1. Difference in the computed ground state energy with respect to monoclinic HfO_2.

which, in turn, leads to oxide trapped charges in electronic devices, causing performance degradation and eventual failure.

In a thin film, HfO_2 multiple phases can coexist within a single grain.[5] Each phase shows different properties, e.g., dielectric constant changes from ∼22 (for the *m*-phase) to ∼50 (for the *t2*-phase).[1] However, it is not clear how the defect formation energy changes across those phases. Since the device reliability is directly related to the material defects, a thorough comparison is important. Many computational studies on *m*, and some on *c* as well as *t* phases, had been previously reported.[6–10] But they do not cover all possible allotropes and their computational methodology differs from each other making a fair comparison difficult.

Electrical characterization on thin film samples gives convoluted data from all the phases present in the sample. Therefore, a comprehensive study of the point defects in each of the phases at the same computational level is necessary. In this paper, we present a density functional theory (DFT) study of different possible point defects in nine lowest energy crystallographic phases of HfO_2.[11] We also model Bias Temperature Instability (BTI)-like electrical measurements with COMPHY [from "nonradiative multi-phonon (NMP) theory"][12] to extract parameters defining the shallow defect band in 10 nm polyphase HfO_2. Finally, we compare both computational and experimental results.

II. COMPUTATIONAL METHODOLOGY

Defect formation in a crystal is a chemical process. The chemical reaction for the formation of vacancy (V) defect is as follows:

$$HfO_2 \rightarrow HfO^{q}_{2\,(V_X)} + X. \quad (1)$$

For interstitial (i) defect formation,

$$HfO_2 \rightarrow HfO^{q}_{2\,(X_i)} - X. \quad (2)$$

Here, $HfO^{q}_{2\,(V_X)}$ and $HfO^{q}_{2\,(X_i)}$ are the defective hafnia system, V_X implies the vacancy of element X, X_i implies an element X that occupies an interstitial site, and q is the charge that the defect acquires. X is a constituent element of hafnia, i.e., either Hf or O. Taking the electronic charge as unit, a defect can acquire +/−1 charge if it lacks/captures one electron and +/−2 for two electrons. Generally, there are two different oxygen sites present in HfO_2: one is threefold coordinated and the other is fourfold coordinated by Hf. Vacancies in such oxygen sites are marked as V_{o3} and V_{o4}, respectively. The formation energy of a defect is the Gibbs free energy, given by[6,13–16]

$$\Delta G = \sum \text{Energy of products} - \sum \text{Energy of reactants}. \quad (3)$$

When the point defect is charged, the total energy of the defective crystal must account for the electrostatic energy "qE_F" in addition to the quantum mechanical ground state energy of the crystal. Here, E_F is the electron chemical potential or the Fermi level of the system with respect to the valence band maximum E_V. The ground state energies of all the reaction products as well as reactants are calculated by solving the Schrödinger equation using density functional theory (DFT). We focus on comparing the allotropes at the same computational level, hence, we use generalized gradient approximation (GGA). From different available GGA functionals, we use Perdew–Burke–Ernzerhof (PBE) as implemented in the CP2K code. Goedecker, Teter, and Hutter pseudopotentials were used for the core 1s, 2s, 2p, 3s, 3p, 3d, 4s, 4p, 4d electrons of Hf and 1s of O.[17] Note that single trapped charge (±1) in the defect centers can show magnetic properties and can lead to energy degeneracy lift-up due to the spin–orbit interaction. To deal with it properly, we use the spin unrestricted Kohn–Sham method. Energy calculations of both bulk and defective hafnia crystal are performed in a 96 atom supercell. A single point defect (vacancy or interstitial) is introduced in the supercell. Afterward, the atomic positions were relaxed for the various charge states of the defects. This step is necessary as a defective crystal undergoes a structural change every time the defect changes the charge state.[10] Finally, the ground state energy of the relaxed system is computed using the Monkhorst–Pack k-point mesh. As energies computed from $2\times2\times2$ and $4\times4\times4$ k-point mesh scheme are found not to differ significantly (in the order of 10 μeV/atom), we used $2\times2\times2$, since it is computationally less costly. Note that if the supercell used in the DFT calculation is not large enough, the methodology underestimates the ground state energy. It is because an image charge appears in the k-space when a Fourier transform of the charged crystal in real space is taken. The interaction of the charge images introduces spurious potential energy in the system that we corrected in our calculation with a FNV scheme.[18]

The energy of an element X is given by its chemical potential μ_X. It is not constant and depends on the concentration of X in the reaction/chemical environment. In this regard, a reaction environment can either be Hf-rich or O-rich. Energy of an oxygen atom is taken to be half of the energy of the oxygen molecule in its triplet state (i.e., the ground state for the molecule). This energy corresponds to the highest value of the chemical potential of oxygen, which occurs in an O-rich system: $\mu_O^{\text{O-rich}}$. Likewise, for Hf in Hf-rich system, $\mu_{Hf}^{\text{Hf-rich}}$ is taken as 1/36th of the bulk energy that is calculated in 36 atom supercell using the

$7 \times 7 \times 7$ Monkhorst–Pack k-point mesh.[6] After computing these values, the lowest limit of the chemical potentials is calculated from the formation energy of defect-free bulk HfO_2, whose formation reaction is

$$\mathrm{Hf} + 2\mathrm{O} \rightarrow \mathrm{HfO_2}. \tag{4}$$

Application of Eq. (3) on this reaction gives

$$\mu_{\mathrm{O}}^{\text{Hf-rich}} = \frac{1}{2}(E[\mathrm{HfO_2}] - E[\mathrm{Hf}]), \tag{5}$$

$$\mu_{\mathrm{Hf}}^{\text{O-rich}} = E[\mathrm{HfO_2}] - 2E[\mathrm{O}], \tag{6}$$

where $E[i]$ is the energy of an element/compound i, i.e., $E[\mathrm{Hf}] = \mu_{\mathrm{Hf}}^{\text{Hf-rich}}$ and $E[\mathrm{O}] = \mu_{\mathrm{O}}^{\text{O-rich}}$. Free energy is given by $\Delta G = \mathrm{dH\text{-}TdS}$, where $H = E + pV$. H, T, S, p, and V are enthalpy, temperature, entropy, pressure, and volume of the system, respectively. As we disregard entropy, pressure, and volume dependency, ΔG in Eq. (3) becomes ΔE, which is given by

$$\Delta E_{(V_X)/(X_i)} = \{E[\mathrm{HfO}^{q}_{2\,(V_X)/(X_i)}] + q(E_V + E_F) \pm \mu_X\} - E[\mathrm{HfO_2}] + E_{\mathrm{Corr}},$$
$$\mu_{\mathrm{Hf}}^{\text{O-rich}} \le \mu_{\mathrm{Hf}} \le \mu_{\mathrm{Hf}}^{\text{Hf-rich}}, \tag{7}$$
$$\mu_{\mathrm{O}}^{\text{Hf-rich}} \le \mu_{\mathrm{O}} \le \mu_{\mathrm{O}}^{\text{O-rich}},$$

where $X = \mathrm{Hf}$ or O. Looking at Eqs. (1) and (2), the positive and negative signs before μ_X are used for vacancy and interstitial defect, respectively. The image charge correction E_{Corr} values are calculated using the FNV method.[18]

The concentration of defects of type "D" with charge "q" in a crystal in the thermodynamic equilibrium is given by[19]

$$C = N\frac{\exp\left(\frac{-\Delta E_D^q}{kT}\right)}{1 + \sum_{q'} \exp\left(\frac{-\Delta E_D^{q'}}{kT}\right)}. \tag{8}$$

Here, N is the number of sites per unit volume of material where a defect can form, k is Boltzmann's constant, and T is the temperature. At low temperature limits, the formula reduces to[20]

$$c = Ne^{\frac{-\Delta E_D^q}{kT}}. \tag{9}$$

Each of them can serve as a charge trapping center that can capture/emit electrons, making the defects charged. A defect reaches an equilibrium charge state for which the Gibbs free energy is minimum (ground state). Transition from charge state q_1 to q_2 can be accomplished by optical, thermal, or combined excitation. The optical transition can temporarily push the system out of equilibrium.[20] The excess energy is dissipated into the lattice as heat (phonons), eventually bringing the system to thermal equilibrium with charge q_2. To calculate the amount of energy lost in the form of heat (relaxation energy), we take the ground state lattice structure (i.e., atomically relaxed system) of HfO_2 at q_1. We put q_2 charge in that and subsequently perform atomic relaxation. Relaxation energy is given by the difference between the initial and the final energy of the atomic relaxation process.

A thermodynamic transition between charge q_1 and q_2 occurs at the Fermi level for which the formation energy of q_1 is equal to that of q_2.[20] Since it is an equilibrium phenomenon, the transition level is also called the "thermal transition level," E_{th}, which is given by

$$E_{th} = \frac{1}{q_2 - q_1}\{E[\mathrm{HfO}^{q_1}_{2\,(V_X)/(X_i)}] - E[\mathrm{HfO}^{q_2}_{2\,(V_X)/(X_i)}] + E_v(q_1 - q_2)\}. \tag{10}$$

III. RESULTS AND DISCUSSION

Values for formation energy can vary depending on the computational methodology used. For example, the chemical potential of the oxygen atom (in O-rich environment) can be taken as the total energy of an isolated atom or as half of the energy of the oxygen molecule at the triplet state. For these two cases, Scopel *et al.* found the formation energy of neutral V_{o4} in m-HfO_2 to be 9.34 eV and 6.40 eV, respectively.[21] Foster *et al.* took the former case and obtained 9.34eV,[4] whereas in our calculation taking the later option, we obtained 6.435 eV. Note that both Scopel *et al.*and Foster *et al.* used plane wave basis, whereas we used localized orbital basis. In addition, Foster *et al.* did not use any image charge correction, which may explain the 0.035 eV difference in the formation of energy values. Table I lists and Fig. 2 shows the formation

TABLE I. Formation energy in eV of different point defects in various crystallographic phases of HfO_2 at charge neutral state.

		Formation energy at zero charge (eV)				
		V_{o3}	V_{o4}	V_{Hf}	Hf_i	O_i
$P2_1/C$	Hf- rich	1.003	1.095	17.262	5.121	7.155
(m)	O- rich	6.435	6.527	6.397	15.985	1.723
Pbca	Hf- rich	1.03	1.113	16.956	5.287	7.168
($o1$)	O- rich	6.45	6.532	6.117	16.125	1.748
Pbca	Hf- rich	0.846	1.138	16.482	6.27	8.045
($o2$)	O- rich	6.25	6.542	5.674	17.078	2.641
$Pca2_1$	Hf- rich	0.861	1.098	17.043	8.304	7.046
($o3$)	O- rich	6.261	6.498	6.243	19.104	1.646
$P4_2/mnm$	Hf- rich	…	1.651	17.312	5.697	9.576
($t1$)	O- rich	…	7.039	6.536	16.472	4.188
$P4_2/nmc$	Hf- rich	0.803	…	17.19	4.436	6.5
($t2$)	O- rich	6.167	…	6.461	15.165	1.136
$Fm\bar{3}m$	Hf- rich	0.856	…	16.264	8.177	6.31
(c)	O- rich	6.169	…	5.638	18.803	0.997
$P2_12_12$	Hf- rich	−1.637	−3.318	12.887	3.089	0.95
($o4$)	O- rich	3.668	1.988	2.276	13.7	−4.356
Pnma	Hf- rich	0.182	0.299	15.768	10.133	7.724
($o5$)	O- rich	5.421	5.538	5.29	20.612	2.484

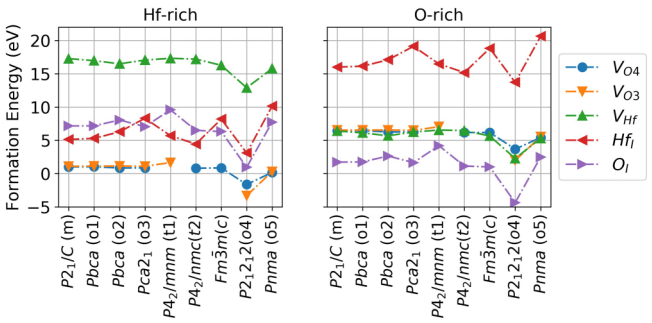

FIG. 2. Comparison of the formation energy of various defects in the neutral charge state.

energy values obtained in our calculations for all five possible types of point defects in their charge neutral state. They are given for two limits of the chemical potential (Hf-rich and O-rich) and for nine crystallographic phases of HfO_2 under study.

Figure 3 shows their formation energy as a function of the Fermi level. The lower limit of the Fermi level $E_F = 0$ corresponds to the valence band maximum. Different crystallographic phases show different defect formation energies for a given defect type. Note that in the *t1* phase, all the oxygen sites are threefold coordinated. Therefore, the *t1* phase does not have any V_{o4} defect. Similarly, all oxygen in *t2* and *c* phases are fourfold coordinated and do not have any V_{o3} defect.

When the chemical environment changes, the formation energy of defects also changes with it as they are interrelated. This leads to a dependence of the oxide's defect concentration (and,

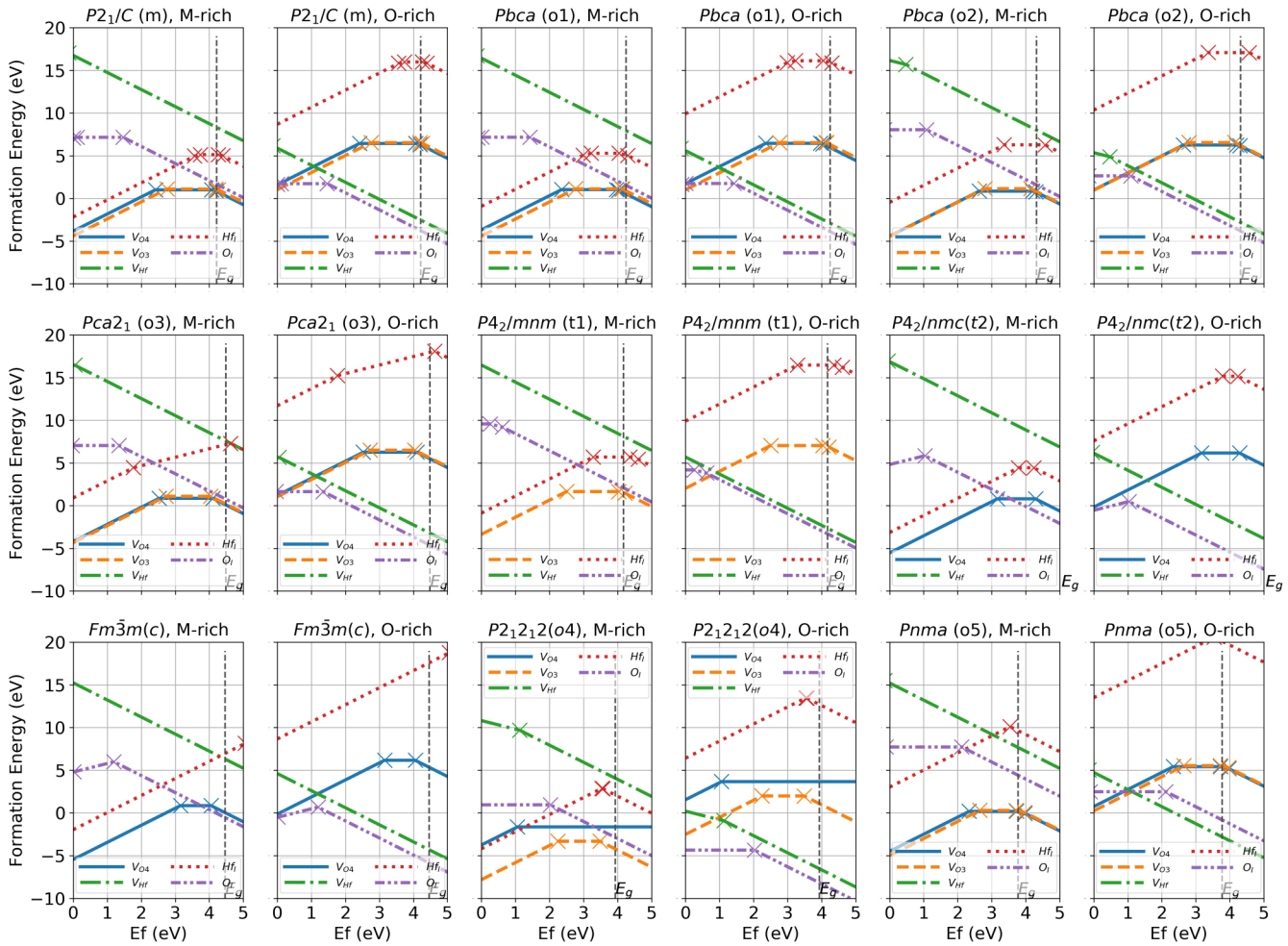

FIG. 3. Formation energy of different point defects in various crystallographic phases of HfO_2. Slope of the lines corresponds to the charge state. Change of slope or the transition from charge q_1–>q_2 is marked by a cross (x). Values of E_f at each transition give the respective E_{th}. V_{Hf} does not show transition from "−2" state within bandgap (except in *o2* and *o4*). *t1* phase does not have V_{o4} defect, *t2* and *c* phases do not have any V_{o3} defect. Top of the valence band is located at 0 eV and bottom of the conduction band is marked by vertical dotted lines.

therefore, its electrical characteristics) on the interface material including the metal electrode, other dielectrics, or semiconductors. Metal electrodes (except Pt) are reactive to oxygen,[22] while the oxygen ions released from the breaking of chemical bonds are sufficiently mobile in HfO_2. Consequently, those metal electrodes scavenge oxygen from HfO_2 and form metal-oxide at the interface. In this process, the interior of HfO_2 becomes O-poor, or in other words, Hf-rich. As a result, hafnia in contact with metals is expected to have oxygen vacancy as a dominant defect. The process is much stronger in highly reactive metals like Ti or Hf while less prominent for relatively inert metals, like Ru or TiN.[23,24] Figures 2 and 3 corroborate this fact, as they show V_{o3} and V_{o4} have low formation energies for all the crystallographic phases in a Hf-rich environment. In addition, owing to the abundance of Hf, Hf_i have low formation energy, while V_{Hf} shows high formation energy. Interestingly, in the *o4* phase, the formation energy of oxygen vacancy in Hf-rich environment is negative. For the O-rich environment, negative formation energy is found for the oxygen interstitial defect (Fig. 2). This means that in such environments, defects will form spontaneously, implying the instability of those phases in those conditions. The chemical environment principles are currently used in applications like resistive RAM, where defects in a dielectric are intentionally created and utilized to create a nonvolatile memory. The charge transition sequence ($q_1 \rightarrow q_2$) is calculated from Fig. 3 by finding the charge state for which Gibbs free energy is minimum at each Fermi level. For example, with increasing the Fermi level, V_{o3} defect of monoclinic goes in the sequence "+2" → "0" → "−1" → "−2" charge state. The system will not find itself in state "+1" as other states are thermodynamically more favorable. Relaxation energy for such transitions for each of the phases and defects is listed in Table II.

Unlike the defect concentration that depends on the formation energy, the thermal transition levels E_{th} are independent of the chemical environment (Hf/O-rich). These levels can be determined experimentally. Figure 4 shows the E_{th} levels of all hafnia phases, for all the defect types, obtained from the DFT calculation. The DFT E_g values underestimate the bandgap. Experimentally obtained bandgap for *m*-HfO_2 is found in the range of 5.25–5.5 eV,[25] while our computation showed 4.21 eV. Table III lists the computed bandgap of all phases. In the lower energy allotropes, i.e., from monoclinic to cubic phases, E_{th} attributed to the oxygen vacancies are located above the midgap while that for interstitial oxygen is located below midgap. In addition, E_{th} of oxygen vacancies show limited variation among different phases compared to other defects. E_{th} for V_{o4} are located between ∼2 eV and ∼0.2 eV below CBM and for V_{o3}, are located between ∼1.5 eV and ∼0.1 eV below CBM (Fig. 4, taking VBM = 0 eV and CBM = E_g, where E_g is the bandgap). For the metal defects, E_{th} from V_{Hf} are located either below VBM or outside of the bandgap. E_{th} for Hf_i are located above VBM, except for the FE *o3*-phase in which it is located slightly below midgap. In fact, E_{th} for both Hf_i and O_i are located close to each other (trap depths are 2.714 and 3.134 eV, respectively). However, their formation energy predicts that for a given chemical environment either of them should be dominant.

To validate the computationally obtained results, we fabricate FETs with undoped HfO_2 and with Si doped HfO_2. They

TABLE II. Relaxation energy (in eV) of different point defects in various crystallographic phases of HfO_2 when it jumps from charge state q_1 to q_2.

			Relaxation energy (eV)				
	q_1	q_2	V_{o3}	V_{o4}	V_{Hf}	Hf_i	O_i
$P2_1/C$	2	0	2.0166	2.5001	0.0846	…	…
(*m*)	2	1	…	…	…	0.2605	0.9014
	1	0	…	…	…	0.2571	0.8431
	0	−1	0.0181	0.0737	0.0186	0.1916	…
	0	−2	…	…	…	…	5.9645
	−1	−2	0.1527	0.1263	0.0206	0.1567	…
Pbca	2	0	2.0003	2.5044	…	…	…
(*o1*)	1	0	…	…	…	0.2455	0.3882
	0	−1	…	0.1597	0.019	0.0111	…
	0	−2	0.3742	…	…	…	6.0062
	−1	−2	…	0.1957	0.0206	0.1890	…
Pbca	2	0	2.0145	2.3472	…	1.4267	…
(*o2*)	2	−1	…	…	3.2743	…	…
	0	−1	…	0.0539	…	…	…
	0	−2	0.5046	…	…	0.0399	6.7969
	−1	−2	…	0.1365	0.1374	…	…
$Pca2_1$	2	0	2.0812	2.4177	…	…	…
(*o3*)	1	−2	…	…	6.5677	0.3434	…
	0	−2	0.9363	0.7014	…	…	6.4934
$P4_2/mnm$	2	0	1.9304	…	…	1.0615	…
(*t1*)	0	−1	0.0289	…	…	0.0167	0.5685
	−1	−2	0.0579	…	0.0115	0.0154	0.4883
$P4_2/nmc$	2	0	…	2.5407	…	1.7267	…
(*t2*)	1	−2	…	…	…	…	6.6847
	0	−1	…	…	0.0188	…	…
	0	−2	…	1.3623	…	2.3875	…
	−1	−2	…	…	0.0282	…	…
$Fm\bar{3}m$	2	1	…	…	…	…	2.9974
(*c*)	2	0	…	0.0168	…	…	…
	2	−1	…	…	…	2.2316	…
	1	−2	…	…	…	…	7.7920
	0	−2	…	4.255	…	…	…
	−1	−2	…	…	…	2.7716	…
$P2_12_12$	2	0	2.7473	…	…	…	…
(*o4*)	2	−1	…	…	…	1.9021	…
	0	−2	0.7874	0.5369	…	…	6.1114
	−1	−2	…	…	0.2003	0.2203	…
Pnma	2	0	1.5489	1.8347	…	…	…
(*o5*)	0	−1	0.0118	0.0107	0.0055	…	…
	0	−2	…	…	…	…	0.0443
	−1	−2	0.0113	0.0117	0.0076	…	…

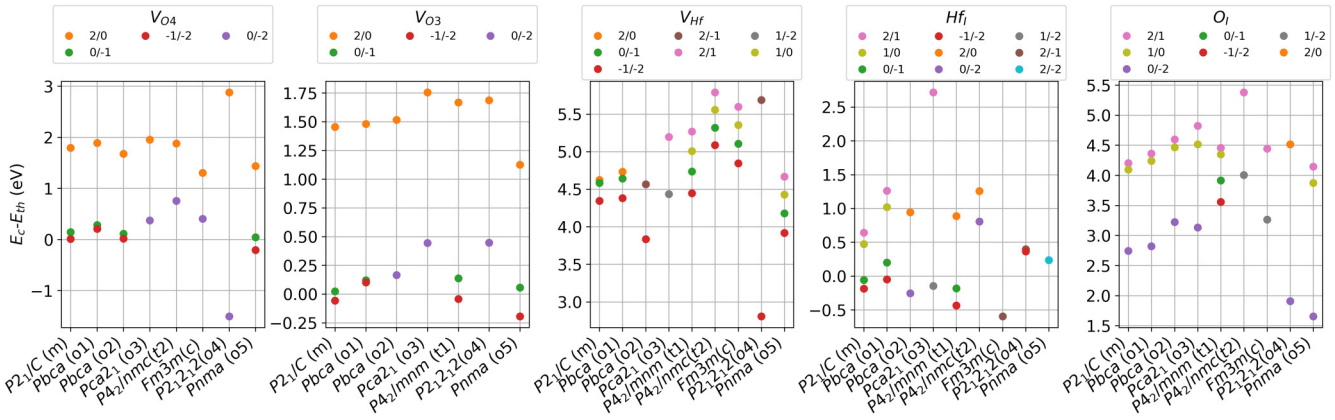

FIG. 4. Charge transition level of point defects with respect to HfO_2 conduction band minimum "E_c" (trap depth), shown for various crystallographic phases of HfO_2.

dominantly possess monoclinic and orthorhombic (FE *o3*) phases, respectively. The latter is confirmed by polarization-voltage measurements that showed ∼4 V coercive voltage and ∼20 μC/cm^2 remnant polarization.[26] Afterward, their trap depth is extracted using the NMP method as shown in Fig. 5 using COMPHY.[12] The tool can detect shallow and midgap traps (attributed to O-vacancies and/or Hf-interstitial) as well as deep traps (attributed to Hf-vacancy and/or O-interstitial). In addition, it can identify whether the defect is located in interfacial oxide or in high-k. Details of the measurement and extraction can be found elsewhere.[26] It may be noted that this method characterizes the thermodynamic transition energy not the optical counterpart. The trap depth of both *m* and *o3* phases are found to be distributed around 1.75 eV. This observation suggests that the sample contains oxygen vacancies as dominant defects. In addition, electrical measurement captured an average value of the trap depth attributed for V_{o4} and V_{o3} defect whose computed trap depths are ∼2 eV and ∼1.5 eV, respectively (Fig. 4). It is because the formation energy for V_{o4} and V_{o3} are almost the same in both *m* and *o3* phases (Fig. 3). That causes both defect types to be present in approximately equal concentrations. Electrical measurement detects the ensemble response which, in turn, gives the mean value of the defect parameters (concentration and trap-depth). The distribution/spread in the measured trap depth most probably is coming from the phase mixture present in the HfO_2 thin film. Figure 4 also suggests that "2/0" trap depth for oxygen vacancies in the *o3*-phase should be located 109 meV above that of the *m*-phase. This range lies within the error bar of the electrical measurement techniques, therefore, cannot be accurately identified.

For several crystalline phases that we reported here, we could not find any reports in the literature. In the present analysis, we show at the same level of theory that V_O in different allotropes is located within a small energy window. The shallow (0.1–1 eV) traps could be coming from the V_O (0/−1),(0/−2) levels, deeper traps (1.2–2 eV) can be ascribed to (2/0) charge transition levels, whereas the deep levels (2.75–3.25 eV deep) can be due to O_i defects (Fig. 4).

The presented results depend on the chosen DFT parameterization, and a further improvement toward higher accuracy results would imply a higher level of theory, which could be expected to improve on the bandgap calculation, albeit at a higher cost. However, we expect the charge-transition levels picture to not change significantly compared to the presently computed PBE values.[27]

TABLE III. Computed bandgap in eV of HfO_2 allotrops under study.

Allotrope	$P2_1/C$ (*m*)	Pbca (*o1*)	Pbca (*o2*)	$Pca2_1$ (*o3*)	$P4_2/mnm$ (*t1*)
E_g (eV)	4.214	4.251	4.315	4.484	4.177
Allotrope	$P4_2/nmc$ (*t2*)	$Fm\bar{3}m$ (*c*)	$P2_12_12$ (*o4*)	Pnma (*o5*)	
E_g (eV)	5.047	4.465	3.937	3.776	

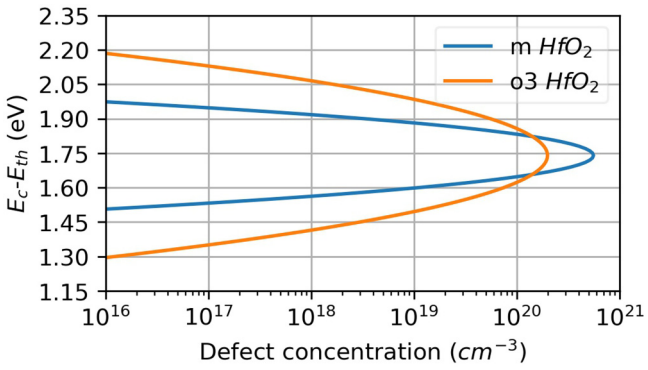

FIG. 5. Measured trap depth in HfO_2 and Si doped HfO_2 using nonradiative multi-phonon theory and COMPHY.

IV. CONCLUSION

Hafnia shows many allotropes with different material properties. This large variation in material properties promises many applications of hafnia materials. The point-defect that is present in the crystal depends on the chemical environment/interface material. In addition, the defect ionization energy depends on the specific allotrope in use. The trap depth for oxygen vacancies, the dominant defect of HfO_2, for all allotropes lies within a small energy window within the bandgap. This observation can be used as a guideline for engineering HfO_2 based devices.

ACKNOWLEDGMENTS

Financial support from EU H2020-NMBP-TO-IND-2018 Project "INTERSECT" (Grant No. 814487) is acknowledged.

DATA AVAILABILITY

The data that support the findings of this study are available from the corresponding author upon reasonable request.

REFERENCES

[1]M. H. Park *et al.*, "A comprehensive study on the structural evolution of HfO_2 thin films doped with various dopants," J. Mater. Chem. C **5**, 4677–4690 (2017).
[2]S. Mueller *et al.*, "Incipient ferroelectricity in Al-doped HfO_2 thin films," Adv. Funct. Mater. **22**, 2412–2417 (2012).
[3]G. He, Z. Sun, G. Li, and L. Zhang, "Review and perspective of Hf-based high-k gate dielectrics on silicon," Crit. Rev. Solid State Mater. Sci. **37**, 131–157 (2012).
[4]A. S. Foster, F. Lopez Gejo, A. L. Shluger, and R. M. Nieminen, "Vacancy and interstitial defects in hafnia," Phys. Rev. B **65**, 174117 (2002).
[5]E. D. Grimley, T. Schenk, T. Mikolajick, U. Schroeder, and J. M. LeBeau, "Atomic structure of domain and interphase boundaries in ferroelectric HfO_2," Adv. Mater. Interfaces **5**, 1701258 (2018).
[6]A. F. Kohan, G. Ceder, D. Morgan, and C. G. Van de Walle, "First-principles study of native point defects in ZnO," Phys. Rev. B **61**, 15019–15027 (2000).
[7]K. Xiong and J. Robertson, "Point defects in HfO_2 high K gate oxide," Microelectron. Eng. **80**, 408–411 (2005).
[8]P. McIntyre, "Bulk and interfacial oxygen defects in HfO2 gate dielectric stacks: A critical assessment," ECS Trans. **11**, 235 (2007).
[9]R. K. Pandey, R. Sathiyanarayanan, U. Kwon, V. Narayanan, and K. V. R. M. Murali, "Role of point defects and HfO_2/TiN interface stoichiometry on effective work function modulation in ultra-scaled complementary metal-oxide-semiconductor devices," J. Appl. Phys. **114**, 034505 (2013).
[10]C. Tang and R. Ramprasad, "Point defect chemistry in amorphous HfO_2: Density functional theory calculations," Phys. Rev. B **81**, 161201(R) (2010).
[11]See https://materialsproject.org for the crystal structure, symmetry group, and other material properties of the allotropes under study.
[12]G. Rzepa *et al.*, "Comphy—A compact-physics framework for unified modeling of BTI," Microelectron. Reliab. **85**, 49–65 (2018).
[13]C. Freysoldt *et al.*, "First-principles calculations for point defects in solids," Rev. Mod. Phys. **86**, 253–305 (2014).
[14]S. B. Zhang, S. H. Wei, and A. Zunger, "Intrinsic n-type versus p-type doping asymmetry and the defect physics of ZnO," Phys. Rev. B **63**, 075205 (2001).
[15]D. B. Laks, C. G. Van de Walle, G. F. Neumark, P. E. Blöchl, and S. T. Pantelides, "Native defects and self-compensation in ZnSe," Phys. Rev. B **45**, 10965 (1992).
[16]A. García and J. E. Northrup, "Compensation of p-type doping in ZnSe: The role of impurity-native defect complexes," Phys. Rev. Lett. **74**, 1131–1134 (1995).
[17]C. Hartwigsen, S. Goedecker, and J. Hutter, "Relativistic separable dual-space Gaussian pseudopotentials from H to Rn," Phys. Rev. B **58**, 3641.
[18]C. Freysoldt, J. Neugebauer, and C. G. Van De Walle, "Fully *ab initio* finite-size corrections for charged-defect supercell calculations," Phys. Rev. Lett. **102**, 016402 (2009).
[19]M. Youssef and B. Yildiz, "Intrinsic point-defect equilibria in tetragonal ZrO_2: Density functional theory analysis with finite-temperature effects," Phys. Rev. B **86**, 1–14 (2012).
[20]C. G. Van de Walle and J. Neugebauer, "First-principles calculations for defects and impurities: Applications to III-nitrides," J. Appl. Phys. **95**, 3851–3879 (2004).
[21]W. L. Scopel, A. J. R. da Silva, W. Orellana, and A. Fazzio, "Comparative study of defect energetics in HfO_2 and SiO_2," Appl. Phys. Lett. **84**, 1492 (2004).
[22]O. Sharia, K. Tse, J. Robertson, and A. A. Demkov, "Extended Frenkel pairs and band alignment at metal-oxide interfaces," Phys. Rev. B **79**, 125305 (2009).
[23]B. Traoré *et al.*, "HfO_2-based RRAM: Electrode effects, Ti/HfO2 interface, charge injection, and oxygen (O) defects diffusion through experiment and *ab initio* calculations," IEEE Trans. Electron Devices **63**, 360–368 (2016).
[24]S. Clima *et al.*, "First-principles thermodynamics and defect kinetics guidelines for engineering a tailored RRAM device," J. Appl. Phys. **119**, 225107 (2016).
[25]M. C. Cheynet, S. Pokrant, F. D. Tichelaar, and J. L. Rouvière, "Crystal structure and band gap determination of HfO_2 thin films," J. Appl. Phys. **101**, 054101 (2007).
[26]B. J. O. Sullivan *et al.*, "Defect profiling in FEFET Si: HfO_2 dielectric layers," Appl. Phys. Lett. **117**, 203504 (2020).
[27]H. Zhu, C. Tang, L. R. C. Fonseca, and R. Ramprasad, "Recent progress in *ab initio* simulations of hafnia-based gate stacks," J. Mater. Sci. **47**, 7399–7416 (2012).